ACS OMEGA

http://pubs.acs.org/journal/acsodf

Article

Properties and Morphologies of Anion-Exchange Membranes with Different Lengths of Fluorinated Hydrophobic Chains

Yuto Shirase, Akinobu Matsumoto, Kean Long Lim, Donald A. Tryk, Kenji Miyatake,* and Junji Inukai*

Cite This: *ACS Omega* 2022, 7, 13577−13587

Read Online

ACCESS | Metrics & More | Article Recommendations | Supporting Information

ABSTRACT: An anion-exchange electrolyte membrane, QPAF(C6)-4, polymerized with hydrophobic 1,4′-bis(3-chlorophenyl)perfluorohexane and hydrophilic (6,6′-(2,7-dichloro-9*H*-fluorene-9.9-diyl)bis(*N*,*N*-dimethylhexan-1-amine) is physically flexible and chemically stable. The drawbacks are relatively large water swelling and lower OH^- conductivity at higher water uptakes, which are considered to be due to the entanglement of the flexible hydrophobic structure of the membrane. In this study, a QPAF(C4)-4 membrane was newly synthesized with shortened hydrophobic fluoroalkyl chains. Unexpectedly, QPAF(C4)-4 showed a higher water uptake and a lower bulk/surface conductivity than QPAF(C6)-4 possibly due to the decrease in hydrophobicity with a smaller number of fluorine atoms. The thermal stability of QPAF(C4)-4 was higher than that of QAPF(C6)-4, possibly due to the rigidity of the QAPF(C4)-4 structure. A higher mechanical strength of QAPF(C6)-4 than that of QPAF(C4)-4 could be explained by the larger interactions between molecules, as shown in the ultraviolet−visible spectrum. The interactions of molecules were understood in more detail with density functional theory calculations. Both the chemical structures of the polymers and the arrangements of the polymers in the membranes were found to influence the membrane properties.

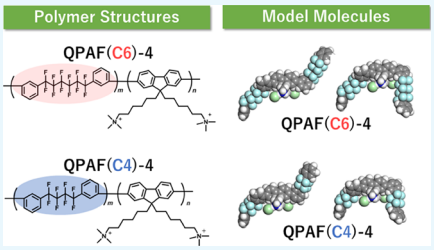

1. INTRODUCTION

Fuel cells, having high efficiency and low emissions, are attracting much attention as clean energy conversion devices.[1,2] Proton-exchange membrane fuel cells (PEMFCs) have already been commercialized to be used for automobile and residential uses. Recently, anion-exchange membrane fuel cells (AEMFCs) have been intensively investigated because of the potential use of nonprecious metal catalysts, such as Pt, as well as the enhanced oxygen reduction reaction kinetics on catalysts under alkaline conditions.[3−10] The challenge of AEMFCs for practical applications is to achieve both high performance and durability. In particular, ion conductivity and chemical/mechanical durability of anion-exchange membranes (AEMs), especially at high temperatures under harsh alkaline conditions, need to be further improved. For enhancing the performance of AEMs, many polymer backbone structures[11−19] and cation-exchange head groups[20−25] have been studied and proposed. AEM side chains,[26−29] OH^- ion transport,[28,30−32] and alkali stability[33−36] have also been investigated. Our group has proposed a series of poly(arylene perfluoroalkylene) copolymers with benzyl-type quaternary ammonium groups (QPAFs, Figure 1).[37−44] The partially fluorinated chemical structures brought about distinct phase-separated nanometer structures, resulting in high anion conductivity, which were caused by the different hydrophilic and hydrophobic moieties in the polymers. The mechanical strength of the polymer membranes also increased by the introduction of perfluoroalkylene groups. QPAF(C6)-4 (Figure 1a) with pendant ammonium head groups was more recently designed for better alkaline stability.[43,44] The QPAF(C6)-4 membrane exhibited high OH^- conductivity (86 mS cm^{-1}) in pure water at 80 °C and superior durability for 1000 h in 1 M KOH solution at 80 °C. The membranes with high ion-exchange capacity (IEC) over 1.5 meq. g^{-1} exhibited large water absorption causing lower OH^- conductivity and dimensional/mechanical instability.[44] The large water absorption was considered to be due to the entanglement of the flexible hydrophobic structure of the membrane.[44]

We have newly synthesized QPAF(C4)-4 (Figure 1b) with a shortened length of the perfluoroalkylene group in the hydrophobic structure of QPAF(C6)-4. In this study, we investigated the effects of the smaller number of fluorine atoms and the different interactions of the aromatic hydrophobic groups in QPAF(C4)-4 on the morphology and properties of the membrane.

2. RESULTS AND DISCUSSION

2.1. Synthesis of 1,4-Bis(3-chlorophenyl)-perfluorobutane (PAF(C4)). PAF(C4) was synthesized, as shown in Scheme 1. To confirm the chemical structures of PAF(C4), nuclear magnetic resonance (NMR) measurements

Received: December 9, 2021
Accepted: March 30, 2022
Published: April 12, 2022

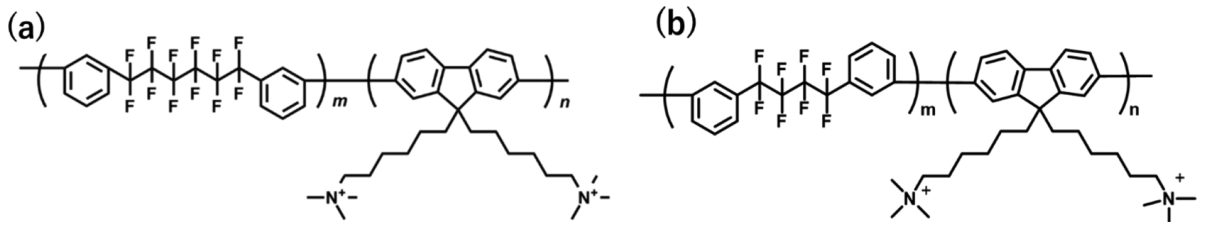

Figure 1. Chemical structures of QPAF(C6)-4 (a) and QPAF(C4)-4 (b).

Scheme 1. Synthesis of (1,4-Bis(3-chlorophenyl)perfluorobutane: PAF(C4))

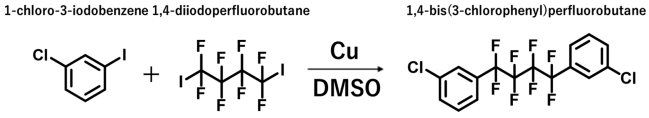

of ^{19}F and ^{1}H were carried out. The spectrum of PAF(C4) is shown as a typical example in Figure 2. All the peaks were well-assigned to the proposed chemical structure.

2.2. Synthesis of QPAF(C4)-4 Copolymers and Membranes. The copolymers of QPAF(C4)-4 were synthesized, as shown in Scheme 2. The series of copolymers, PAF(C4)-4 with monomer ratios (m and n), was obtained with high molecular weights [number average molecular weight (M_n) = 9 kDa and weight average molecular weight (M_w) = 26 kDa]. The polydispersity indexes (PDI) (M_w/M_n = 2.8) were lower than those of our PAF(C6)-4 (M_w/M_n = 10.2−17.4), sharing the same hydrophilic component.[43,44] The obtained PAF(C4)-4 were soluble in chloroform, DMAc, and dimethyl sulfoxide (DMSO), but not in methanol. To confirm the chemical structures of the PAF(C4)-4 copolymers, NMR measurements of ^{19}F and ^{1}H were carried out. Figure 3 shows the spectrum of PAF(C4)-4. All the peaks were well-assigned to the proposed chemical structure.

The quaternization reaction of PAF(C4)-4 was performed using dimethyl sulfate in DMAc solution. The direct casting from the reaction mixture gave QPAF(C4)-4 membranes in the $MeOSO_3^-$ form, which were yellow, transparent, and mechanically strong. The obtained QPAF(C4)-4 membranes were bendable but less flexible than the QPAF(C6)-4 membranes.[43,44] The chemical structure of QPAF(C4)-4 in the $MeOSO_3^-$ form was confirmed by nuclear magnetic resonance (NMR) spectra of ^{19}F and ^{1}H (Figure 4); the quaternization reaction was ensured by the shift of the methyl and methylene protons attached to the nitrogen atoms to the lower magnetic field compared with those of the precursor PAF(C4)-4. The ratios of integral peaks between 1−7 and 13 and 14 suggested that the quaternization reaction quantitatively proceeded. The values of IEC obtained from titration (2.0 meq. g^{-1}) and from the copolymer compositions of QPAF(C4)-4, or the targeted value (2.1 meq. g^{-1}), were similar. Hereafter, we refer to the titrated IEC values.

2.3. Ultraviolet−Visible Light Absorption Spectroscopy. Figure 5 shows the ultraviolet-visible (UV−vis) light spectra of the QPAF(C4)-4 (blue line) and QPAF(C6)-4 (red line) membranes. The peaks existed at 368 and 366 nm for QPAF(C4)-4 and QPAF(C6)-4, respectively. The spectrum pattern of QPAF(C6)-4 was generally at a higher wavelength than that of QPAF(C6)-4, and the wavelength of QPAF(C6)-4 was broader. Therefore, the interactions between QPAF(C4)-4 polymers are expected to be smaller than those between QPAF(C6)-4 polymers. The interactions between the different polymers were further examined by the following density functional theory (DFT) calculations.

2.4. DFT Calculations. Attention was paid to the hydrophobic units with DFT calculations to see if there were

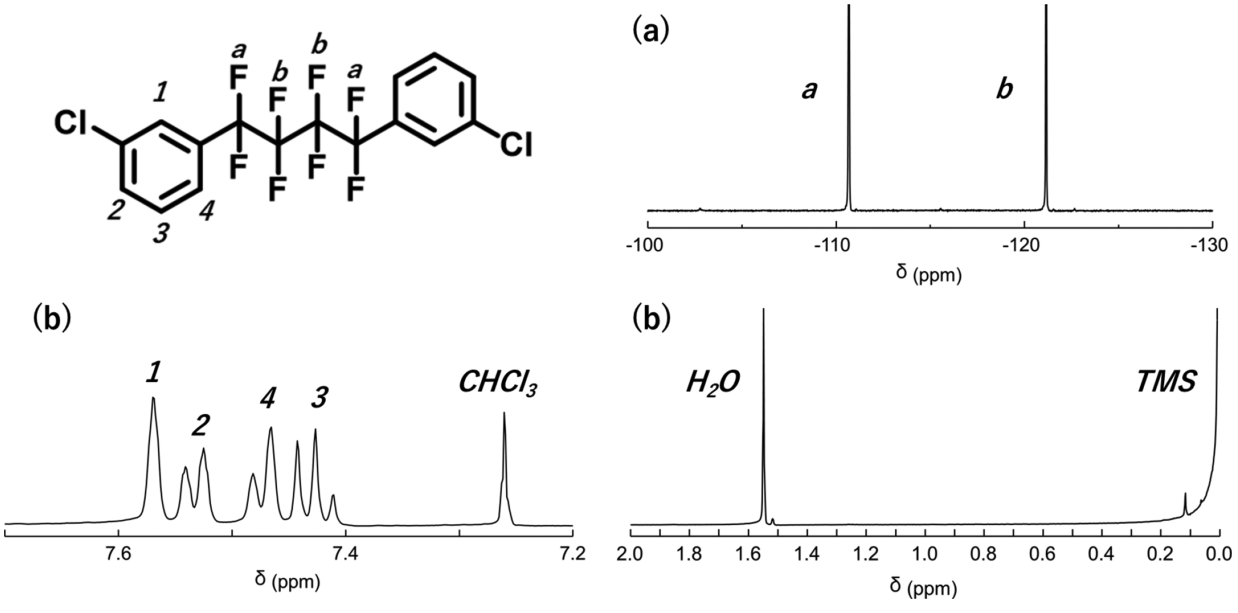

Figure 2. ^{19}F NMR (a) and ^{1}H NMR (b) spectra of 1,4-bis(3-chlorophenyl)perfluorobutane (PAF(C4)) in $CDCl_3$ at room temperature.

https://doi.org/10.1021/acsomega.1c06958
ACS Omega 2022, 7, 13577−13587

Scheme 2. Synthesis of PAF(C4)-4 and QPAF(C4)-4 Copolymers

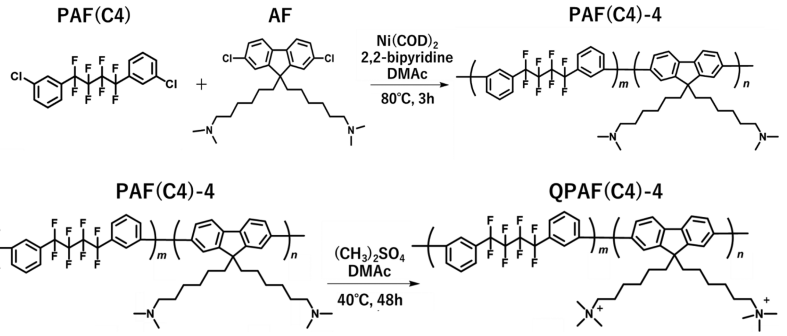

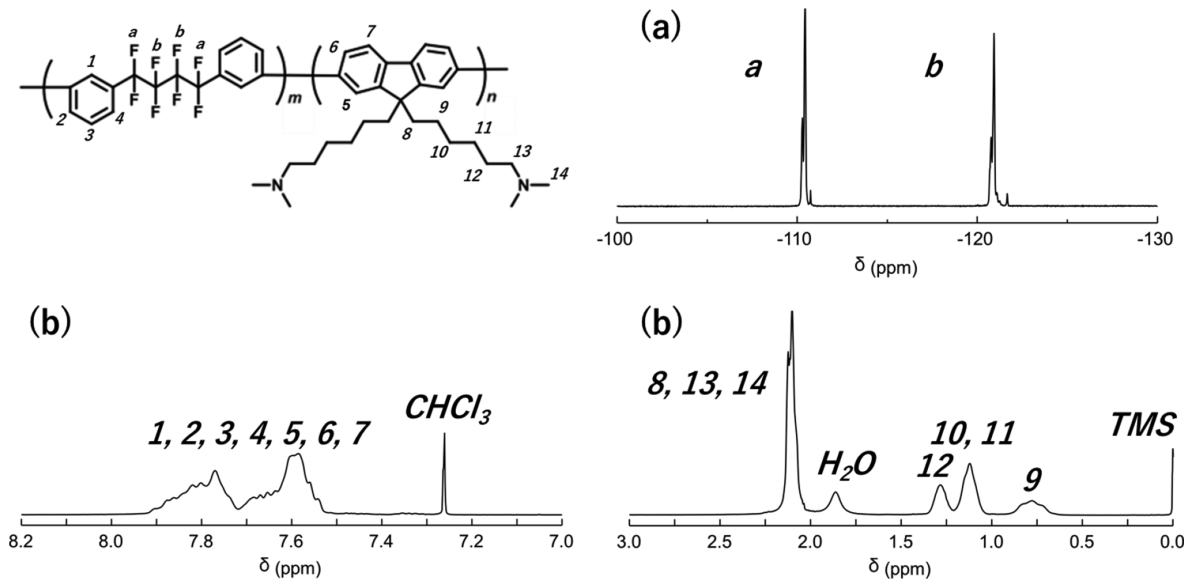

Figure 3. ^{19}F NMR (a) and ^{1}H NMR (b) spectra of PAF(C4)-4 in $CDCl_3$ at room temperature.

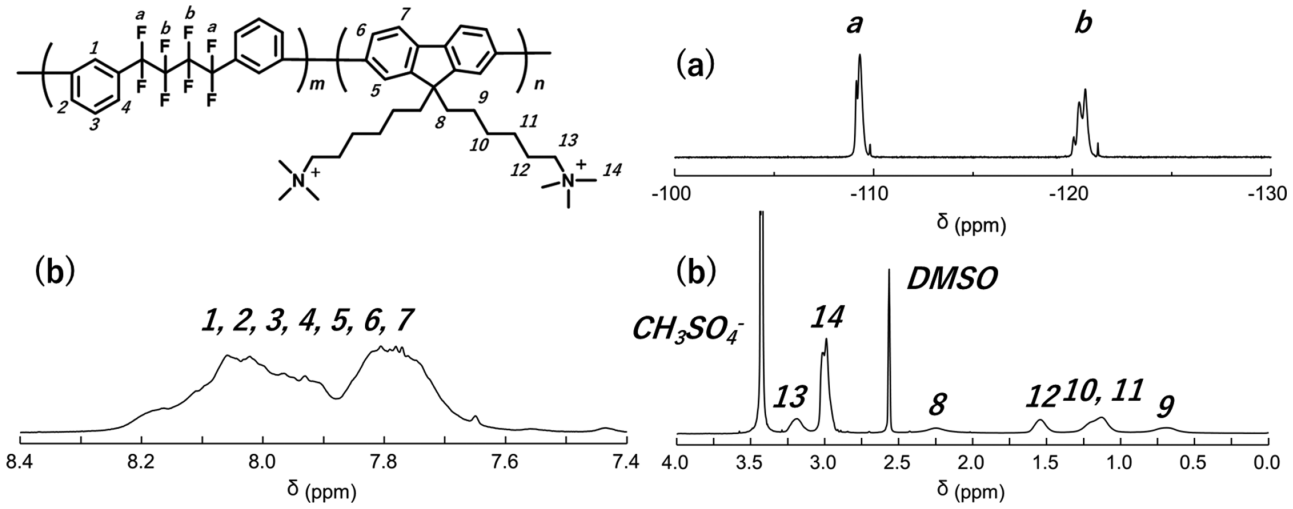

Figure 4. ^{19}F NMR (a) and ^{1}H NMR (b) spectra of QPAF(C4)-4 in DMSO-d_6 at room temperature.

discernable differences in their interactions with each other. Two double units were placed side by side in various orientations (Figure 6a, upper-right structures, and Figure S1 in the Supporting Information) and subjected to molecular dynamics (MD) calculations for 2 ps. The energies are plotted versus time (step number) in Figure 6b. The simulated UV–vis absorption spectra for the final structures are shown in Figure 6c. As shown in Figure 6b, there is a wider range of energies exhibited for the QPAF(C6)-4 hydrophobic units. The spectra (Figure 6c) show that the wavelengths of the peaks λ_{max} were quite variable and generally slightly higher for the QPAF(C6)-4 units. It was generally found that the λ_{max} values were higher when the hydrophobic units were closer together and, more specifically, when the aromatic rings were

https://doi.org/10.1021/acsomega.1c06958
ACS Omega 2022, 7, 13577−13587

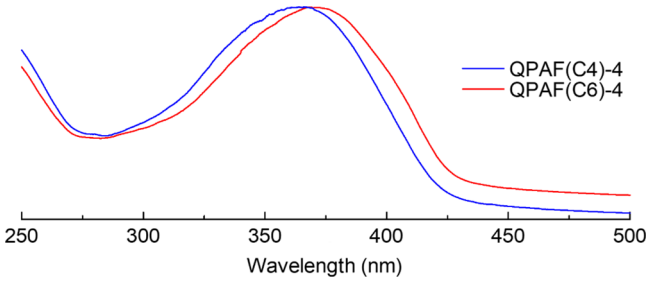

Figure 5. UV-vis spectra of QPAF(C4)-4 (2.0 meq. g^{-1}, blue line) and QPAF(C6)-4 (2.0 meq. g^{-1}, red line).

closer together. It was found that the interactions between the rings on the adjacent units did not have to be either coplanar or stacked as in graphite but could be at any angle to each other. As shown in Figure S2, the λ_{max} values are plotted versus the distances between the closest two hydrogen atoms on neighboring units. Clearly, the correlation is somewhat chaotic, as expected, because the λ_{max} values would depend on a number of factors, but an overall trend can be seen that longer λ_{max} values are associated with smaller H−H distances. The reason that slightly longer λ_{max} values were found for the QPAF(C6)-4 units is most likely to be that the longer perfluoroalkylene chain length allows the neighboring units to have a wider range of motion so that the aromatic rings have a greater probability of approaching each other. By the same token, the wider range of motion also gives the chains the opportunity of being further apart, so that the energies can be larger and even increased (Figure 6b, right panel, blue curve).

Interestingly, however, there was no clear correlation between the energies observed in either the MD runs, the λ_{max} values, or the H−H distances. In the ongoing work, we investigate other types of interactions, other than $\pi-\pi$ interactions between neighboring aromatic rings, to explain the stabilization energies. One possibility is that there are interactions between the perfluoroalkylene chains, as suggested by one of the MD runs for two QPAF(C6)-4 units, seen as the pink curve in Figure 6b (right panel), in which the energy decreased, not because of a short H−H distance but due to the approach of perfluoroalkylene chains (Figure S1, QPAF(C6)-4, 180°). If such an interaction can be confirmed, it could also help to explain some of the physical properties of the QPAF(C6)-4 ionomer.

2.5. Water Uptake and Ion Conductivity. Figure 7a,b shows the water uptake at room temperature and the OH^- conductivity in water at 30 °C, respectively, of the QPAF(C4)-4 and QPAF(C6)-4 membranes. The water uptake of QPAF(C6)-4 increased as the IEC increased. The OH^- conductivity of QPAF(C6)-4 increased as the IEC increased up to IEC = 1.6 meq. g^{-1} and decreased at 2.2 meq. g^{-1}. At IEC = 1.5 and 2.0 meq. g^{-1}, the QPAF(C4)-4 membrane exhibited a higher water uptake but a lower OH^- conductivity than those of the QPAF(C6)-4 membrane. The lower conductivity of QPAF(C4)-4 was explained by the membrane expansion because of excessive water swelling, as evidenced by the comparatively high water uptake values observed (Figure 7a).[44]

Figure 8 shows the temperature dependency of the OH^- conductivity of the QPAF(C4)-4 and QPAF(C6)-4 membranes. The Arrhenius-type dependency was observed on both membranes between 30 and 80 °C. The activation energy (E_a) of OH^- conduction was calculated as 9.7 kJ mol^{-1}, whereas that of QPAF(C6)-4 was 9.8 kJ mol^{-1}.[44] Therefore, the anion conduction mechanism with QPAF(C4)-4 and QPAF(C6)-4 membranes might be similar.

2.6. Mechanical Properties. Figure 9 shows the storage moduli (E') (a) and loss moduli (b) at 60% RH as a function of temperature. The value of E' of the QPAF(C4)-4 membrane showed a decrease around 80 °C, whereas E'' of QPAF(C4)-4 showed a peak around 85 °C. These values were higher than those of the QPAF(C6)-4 membrane. The change in E' was related to its transition temperature, while the change in E'' was related to its mechanical strength. Therefore, shortening the hydrophobic perfluoroalkylene chains contributed to the increase in glass transition temperature and mechanical strength. The improved thermomechanical stability is explained by the increased rigidity associated with the inhibition of the internal rotation of the molecule around the interatomic bond.[45] A higher rigidity of QPAF(C4)-4 was possibly due to a higher ratio of aromatic groups and a lower freedom with shorter perfluoroalkylene chains.

Figure 10 shows stress (or tensile strength) versus strain (or elongation) curves obtained for the QPAF(C4)-4 and QPAF(C6)-4 membranes in the Cl^- form at 80 °C and 60% RH, respectively. On both curves, the initial steep rising portion, indicative of elastic behavior, is followed by a wide region of inelastic elongation, that is, stress relaxation, because both membranes were similarly able to accommodate the expansion. This is a typical behavior for ionomeric membranes.[12,15,21,39,40] However, the QPAF(C6)-4 membrane exhibited larger slopes in both the elastic region (Young's modulus) and the inelastic region, indicating a higher resistance to expansion, which suggests a higher degree of interaction between the polymer chains.

QPAF(C4)-4 showed a maximum stress of 11 MPa and an elongation rate of 150%. QPAF(C6)-4 showed a smaller maximum stress of 8 MPa but a higher elongation rate of 190%. The improved elongation rate was reported to be due to the increased resistance to deformation associated with increased entwinement of polymer chains.[46] A larger entwinement was explained by larger interactions between QPAF(C6)-4 molecules, as confirmed in the UV−vis absorption spectra (Figure 5) and by the DFT and MD calculations (Figure 6). The electronic structures and conformations of molecules are thus linked.

2.7. Morphology of Membranes. To obtain transmission electron microscopy (TEM) images, QPAF(C4)-4 membranes were ion-exchanged from $MeOSO_3^-$ to $PtCl_4^{2-}$. The QPAF-(C4)-4 membranes became reddish brown and less flexible in $PtCl_4^{2-}$ forms. Figure 11 shows cross-sectional TEM images of QPAF(C4)-4 and QPAF(C6)-4 membranes. The dark areas are related to hydrophilic domains containing ion-exchanged ammonium groups and the bright areas to hydrophobic domains composed of the polymer backbones. Both QPAF-(C6)-4 and QPAF(C4)-4 had a spherical hydrophilic domain (approximately 1.5 nm in diameter). The size of the bright hydrophobic domains was also 1.5 nm. The morphology of the QPAF(C4)-4 membrane at the nanometer scale was similar to that of the QPAF(C6)-4 membrane. The influence of shortening the hydrophobic alkyl chain on the phase-separated morphology under vacuum was negligibly small.

The bulk morphology under the humidified conditions was studied using small-angle X-ray scattering (SAXS).[47] The SAXS measurements of the QPAF(C4)-4 (IEC = 2.0 meq. g^{-1}) and QPAF(C6)-4 (IEC = 2.0 meq. g^{-1}) membranes in

https://doi.org/10.1021/acsomega.1c06958
ACS Omega 2022, 7, 13577−13587

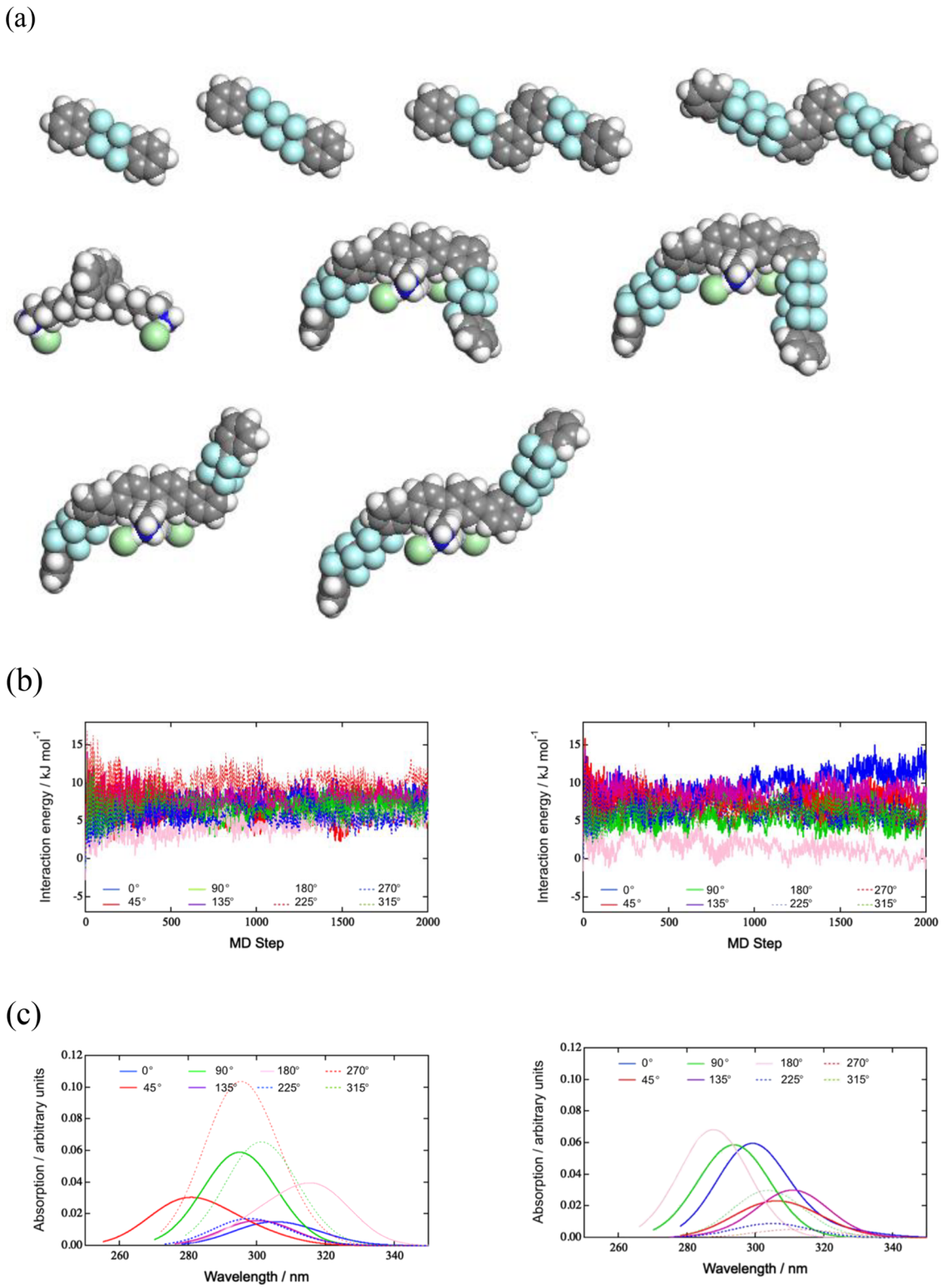

Figure 6. (a) Representative subunits of the QPAF(C4)-4 and QPAF(C6)-4 ionomers used in the present DFT calculations: single hydrophobic units (top row, left), double hydrophobic units (top row, right), hydrophilic unit (second row, left), two hydrophobic units joined by a hydrophilic unit (*cis*-configurations, second row, right and trans configurations, bottom row). (b) MD runs for two double hydrophobic units of QPAF(C4)-4 (left panel) and QPAF(C6)-4 (right panel). Each run consisted of 1 fs per step and a total of 2 ps. The corresponding final structures are depicted in Figure S1. (c) Calculated λ_{max} values for the final MD structures of QPAF(C4)-4 (left panel) and QPAF(C6)-4 (right panel).

the Cl^- form were carried out at 40 °C, changing the RH from 30 to 90%. The scattered intensity was plotted with respect to the scattering vector (q), as shown in Figure 12. For QPAF(C4)-4, a peak existed at around q = 0.8 nm^{-1} or 8 nm of the d spacing, and its position and intensity changed with increasing RH, indicating that the absorbed water was responsible for the development of the periodic structure. The results of QPAF(C6)-4 were nearly the same as those of

https://doi.org/10.1021/acsomega.1c06958
ACS Omega 2022, 7, 13577−13587

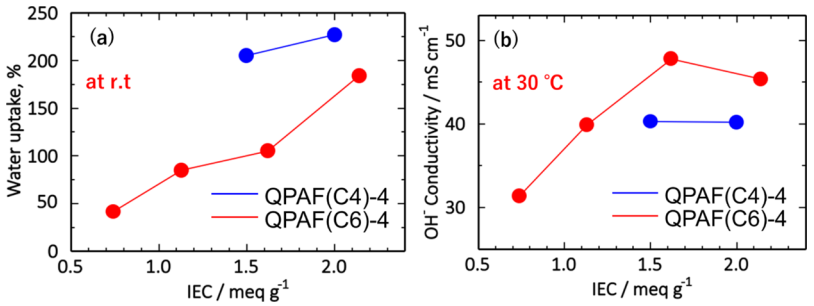

Figure 7. Water uptake at room temperature (a) and OH^- conductivity at 30 °C (b) of QPAF(C4)-4 (red circles) and QPAF(C6)-4 (blue circles) membranes in water as a function of IEC.

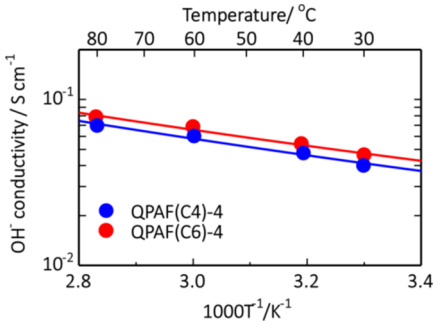

Figure 8. Temperature dependency of the OH^- conductivity of QPAF(C4)-4 (2.0 meq. g^{-1}, blue circles) and QPAF(C6)-4 (2.1 meq. g^{-1}, red circles) membranes.

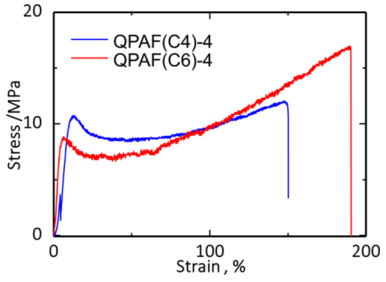

Figure 10. Stress vs strain curves of QPAF(C4)-4 (2.0 meq. g^{-1}, blue line) and QPAF(C6)-4 (2.0 meq. g^{-1}, red line) membranes in the Cl^- form at 80 °C and 60% RH.

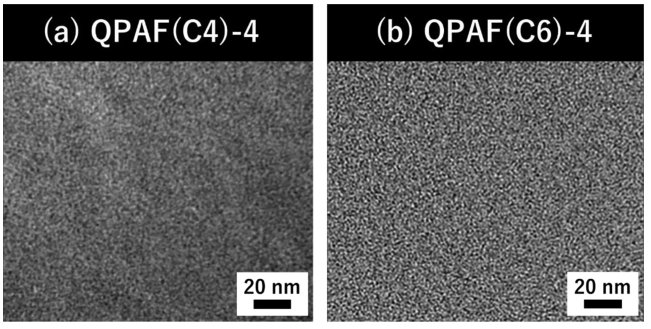

Figure 11. Cross-sectional TEM images of the QPAF(C4)-4 (2.0 meq. g^{-1}) (a) and QPAF(C6)-4 (2.0 meq. g^{-1}) (b) membranes in the $PtCl_4^{2-}$ form.

QPAF(C4)-4, which showed a peak at d = 7 nm at 30% RH (Figure 12b), slightly smaller than the d value of QPAF(C4)-4. The peak developed with an increase in humidity, showing an increase in periodicity.[44]

On the basis of the DFT calculations, atomic-scale differences were proposed between the QPAF(C4)-4 and QPAF(C6)-4. Based on the TEM and SAXS results, no significant differences were reflected in the nanoscale morphology of the bulk materials.

Figure 13 shows the topographic images of QPAF(C4)-4 (a) and QPAF(C6)-4 (b) and the current images of QPAF(C4)-4 (c) and QPAF(C6)-4 (d) obtained by current-sensing atomic force microscopy (CS-AFM).[48−53] The topographic and current images were simultaneously measured. The surface roughness of the QPAF(C4)-4 and QPAF(C6)-4 membranes was approximately 15 nm. On both QPAF(C4)-4 and QPAF(C6)-4, current densities were commonly higher in the current images at the convex positions in the topographic images. On the surfaces of both membranes, the conduction area occupied 99% of the whole surface areas (threshold value: 0.5 pA). The average current and the standard deviation of the QPAF(C4)-4 membrane were 3.6 and 1.3 pA, respectively, whereas those values of QPAF(C6)-4 were 5.2 and 1.4 pA, respectively. Therefore, the surface conduction of QPAF(C4)-4 was lower than that of QPAF(C6)-4. As explained for the

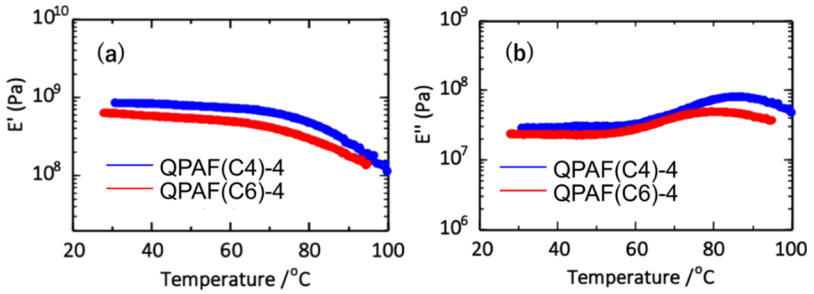

Figure 9. Temperature-dependency curves of storage moduli (E') (a) and loss moduli (E'') (b) of membranes of QPAF(C4)-4 (2.0 meq. g^{-1}, blue lines) and QPAF(C6)-4 (2.0 meq. g^{-1}, red lines) in the Cl^- form at 60% *RH*.

https://doi.org/10.1021/acsomega.1c06958
ACS Omega 2022, 7, 13577−13587

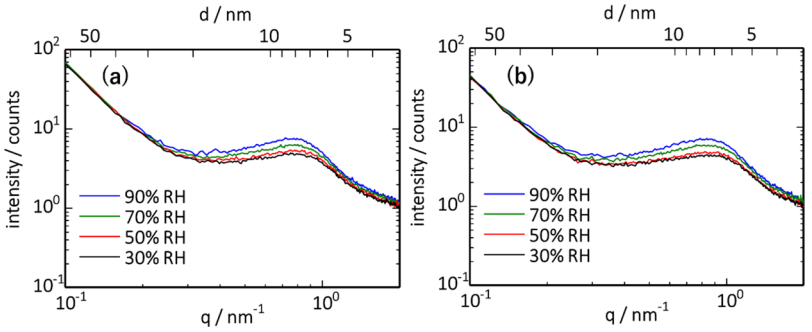

Figure 12. SAXS profiles of the QPAF(C4)-4 (IEC = 2.0 meq. g^{-1}) (a) and QPAF(C6)-4 (IEC = 2.0 meq. g^{-1}) (b) membranes in the Cl^- form as a function of the scattering vector (q) at 40 °C and 30, 50, 70, and 90% RH.

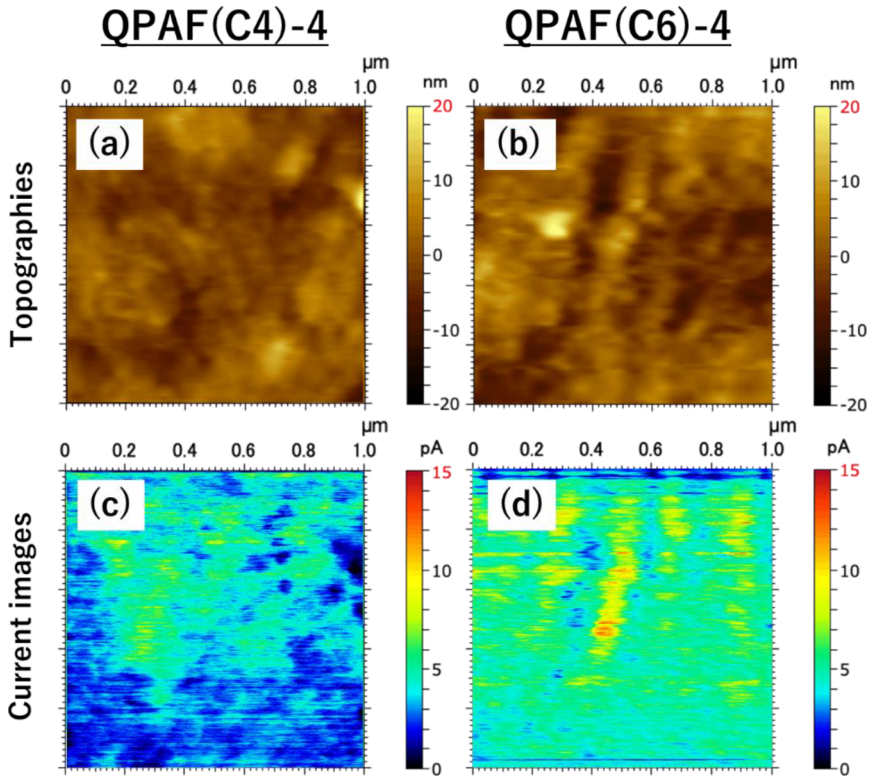

Figure 13. Topographic and current images of QPAF(C4)-4 (IEC = 2.0 meq. g^{-1}) ((a), (c)) and QPAF(C6)-4 (IEC = 2.0 meq. g^{-1}) (b,d) at 40 °C and 70% RH under purified air. Tip bias voltage = −2.0 V. Contact force = 5 nN.

bulk conductivity (Figure 7), this should be also due to a higher water uptake at the surface of QPAF(C4)-4.

In the case of the surface, in contrast to the bulk, differences in the morphology and conduction were clearly observed at the micrometer scale. This is reasonable because of the larger freedom of motion at the surface.

3. CONCLUSIONS

We have developed a novel QPAF(C4)-4 membrane by shortening the hydrophobic perfluoroalkylene chains of QPAF(C6)-4. The UV−vis absorption spectra of the membranes suggested that there was a higher degree of $\pi-\pi$ interactions between polymer chains in the QPAF(C6)-4 membrane than those in the QPAF(C4)-4 membrane, which was consistent with the findings in molecular dynamics calculations, but the latter also pointed to enhanced interactions between the perfluoroalkylene chains of QPAF-(C6)-4 as a stabilizing factor. The QPAF(C4)-4 membrane showed a higher water content than that of QPAF(C6)-4 in accordance with the decrease in the number of hydrophobic fluorines. The conductivity was lower than that of QPAF(C6)-4 in the high IEC region because of excessive water swelling. The QPAF(C4)-4 membrane showed a higher thermal stability but a lower flexibility than those of QPAF(C6)-4. In both membranes, micro-phase-separated structures were clearly developed. The TEM images showed no clear difference between the size of the hydrophilic and hydrophobic domains under dry conditions. According to the SAXS results under humidified conditions, the domain sizes of QPAF(C4)-4 were larger than those of QPAF(C6)-4 because of the increase in water uptake as the number of hydrophobic fluorines decreased. From the CS-AFM measurements, the morphological difference on the surfaces of the QPAF(C4)-4 and QPAF(C6)-4 membranes was small, but the surface conduction of QPAF(C6)-4 was higher than that of QPAF(C4)-4.

https://doi.org/10.1021/acsomega.1c06958
ACS Omega 2022, 7, 13577−13587

In this study, it was demonstrated that the properties of membranes, such as water uptake and thermal/mechanical strength, can be controlled by changing the length of the perfluoroalkylene chains. The mechanism of the improvements was discussed, which could be used to further design anion ionomers.

4. EXPERIMENTAL SECTION

4.1. Synthesis of QPAF(C4)-4. *4.1.1. Synthesis of Monomer (1,4-Bis(3-chlorophenyl)perfluorobutane: PAF-(C4)).* 1,4-Diiodoperfluorobutane (9.98 g, 22 mmol), 1-chloro-3-iodobenzene (15.7 g, 66 mmol), Cu powder (14.0 g, 220 mmol), and DMSO (88 mL) were placed into a three-necked flask (300 mL) with a nitrogen inlet and a mechanical stirrer. After increasing the temperature to 120 °C, the mixture was stirred under nitrogen for 48 h. After stirring, the solution was washed with 500 mL of 0.1 M nitric acid. Subsequently, stirring and filtering with 200 mL of methanol were carried out repeatedly three times to obtain the target solution. The obtained reaction solution was washed with methanol/ultrapure water (500 mL, 3/2, volume/volume) solution three times and dried at 60 °C in a vacuum oven to obtain 2.97 g of 1,4-bis(3-chlorophenyl)perfluorobutane as white fiber in 32% yield.[44]

4.1.2. Polymerization. 1,4-Bis(3-chlorophenyl)-perfluorobutane (PAF(C4)) (1.83 g, 4.32 mmol), 6,6′-(2,7-dichloro-9*H*-fluorene-9.9-diyl)bis(*N*,*N*-dimethylhexan-1-amine (AF) (1.44 g, 2.95 mmol), 2,2′-bipyridine (2.84 g, 18.2 mmol), and *N*,*N*-dimethylacetamide (DMAc) (18 mL) were placed into a three-necked flask (100 mL) with a nitrogen inlet and a mechanical stirrer. The mixture was heated and stirred at 80 °C. Then, bis(cyclooctadiene)nickel(0) (5.00 g, 18.2 mmol) was added into the mixture. Subsequently, the homogeneous mixture was poured into a mixture of methanol and concentrated hydrochloric acid (1:1 by volume, 400 mL) for polymerization to obtain a black precipitate for 3 h at 80 °C. The crude product was filtered, washed with concentrated hydrochloric acid (200 mL), and treated with saturated K_2CO_3 aqueous solution (200 mL). The product was washed with water (200 mL) and dried in a vacuum oven at 60 °C to obtain 2.50 g of 1,4-bis(3-chlorophenyl)perfluorobutane (PAF(C4)-4) (m = 1.00 and n = 0.51 in Figure 1b) as white fiber in 91% yield.

4.1.3. Preparation of QPAF(C4)-4 Membranes. PAF(C4)-4 (2.5 g, 7.88 mmol of dimethylamino groups) and DMAc (16.5 mL) were added into a round-bottom flask (50 mL) with a nitrogen inlet and a mechanical stirrer. Dimethyl sulfate (1.2 mL, 12.6 mmol) was added into the mixture for quaternization of the polymer. The mixture was stirred for 48 h at 40 °C and diluted with DMAc (20.0 mL). The mixture was poured into pure water, dialyzed, evaporated, and dried under vacuum at 60 °C to obtain QPAF(C4)-4 (m = 1.00, n = 0.65) as white fibrous solid in 83% yield. QPAF(C4)-4 (2.0 g) was dissolved in DMAc (40 mL) and then filtered with a syringe stuffed with cotton. The transparent solution was cast onto a flat glass plate. The solution was dried at 40 °C overnight to form a light brown transparent membrane. The resulting membrane was dried at 60 °C under vacuum. By soaking the membrane in 1 M KOH aqueous solution at 80 °C for 48 h, the counter anions were substituted with OH^- ions. The resulting membrane in the OH^- form was washed and immersed in degassed and deionized water for at least 1 day to completely remove excess KOH. QPAF(C4)-4 in the Cl^- form was prepared by immersing the membrane in the hydroxide ion form into 1 M hydrochloric acid for 48 h at room temperature.

4.2. NMR. NMR spectroscopy was carried out with JNM-ECA500 (JEOL) for the determination of the synthesized species. Chloroform-*d* and dimethylsulfoxide-d_6 (DMSO-d_6) were used as deuterated solvents. Tetramethylsilane (TMS) was used as a reference substance.

4.3. Gel Permeation Chromatography. K-805 L (Shodex) was selected as the separation column of gel permeation chromatography. UV-2077 (Jasco) was used as the detector, and the detection wavelength was 270 nm. Chloroform in which 0.02 M triethylamine was dissolved was used as an eluent. The eluent flow rate was 1.0 mL min^{-1}. The calibration curve for the molecular weight was created using standard polystyrene, M_n and M_w of the measured samples were calculated from the obtained calibration curve, and the degree of dispersion was obtained from M_w/M_n.

4.4. IEC Measured by Titration. Mohr's method was used to measure the IEC of the membrane.[54] In an acid−base back-titration, the OH^- from the membrane was treated with excess HCl, and the decrease in the amount of H^+ was measured via titration with NaOH. On the other hand, because Mohr's method uses a Cl^--form membrane, it is not affected by carbon dioxide in the air, and thus, more accurate values can be obtained.

After immersing the dry membrane (Cl^- form) in 12.5 mL of a 0.2 M sodium nitrate aqueous solution, 1.0 mL of a 0.1 M sodium chloride aqueous solution was added, and ion exchange was carried out by stirring overnight. A potassium chromate aqueous solution (1.6 mL) (0.25 M) was added to the obtained solution and stirred. Sodium hydrogen carbonate aqueous solution (1 mL) (0.1 M) was added to make the solution weakly basic. A 0.01 M silver nitrate aqueous solution was added dropwise to the prepared solution using a burette, and the endpoint was defined, at which the yellow solution became slightly reddish. The titration was performed at least 3 times both for the reference and for this measurement, and the values (2.09, 1.98, and 1.93 meq. g^{-1}) were averaged. The IEC was calculated according to eq 1:

$$\mathrm{IEC} = \frac{\text{amount of dropping of silver nitrate aqueous solution (mmol)}}{\mathrm{Cl^-}\text{ form membrane weight (mg)}} \quad (1)$$

4.5. OH^- Conductivity. The sample was cut into 1 cm × 3 cm and attached to a cell for conductivity measurement. The distance between Au probes was 1.0 cm. Conductivity measurements were performed with 1255B/1287 of Solartron, using the AC 4-terminal method (300 mV, 10−100,000 Hz). For impedance, Z, the value at which the phase angle converges to 0° on the board plot was used. The conductivity σ (S cm^{-1}) was calculated by Formula 2.

$$\sigma = \frac{L}{Z} \times \frac{1}{A} \quad (2)$$

4.6. Water Uptake. The water uptake ($\Delta W(\%)$) measurement was measured after the conductivity measurement shown below. From the difference between the water-containing membrane weight (W_{wet}) and the dry membrane weight (W_{dry}) of the membrane, it was calculated using Formula 3.

$$\Delta W(\%) = \frac{W_{wet} - W_{dry}}{W_{dry}} \times 100 \quad (3)$$

https://doi.org/10.1021/acsomega.1c06958
ACS Omega 2022, 7, 13577−13587

The mass of the water-containing membrane was quickly measured after wiping off water droplets on the surface of the sufficiently water-containing film with a pro-wipe or the like. The weight of the dried membrane was weighed after vacuum drying the moistened membrane at 50 °C overnight. Water swelling was not measured because of a large error in measuring the volumes of the membranes.

4.7. Dynamic Viscoelasticity. A membrane was cut out to 0.5 cm × 3 cm, and the dynamic viscoelasticity measurement was carried out using DV-200 (IT Measurement Control). The stored viscoelasticity (E'), loss viscoelasticity (E''), and tan δ at 0−90% RH at a humidity rise rate of 1% min^{-1} were obtained at a constant temperature of 80 °C at a measurement frequency of 10 Hz. The measurements were performed in 3 cycles, and the data in the third cycle were used.

4.8. Tensile Test. A dumbbell-shaped membrane was used for the tensile test using Autograph AGS-J500N (Shimadzu). A tensile test was performed at 80 °C and 60% RH. The maximum stress and the elongation rate were determined with an expansion rate of 10 mm min^{-1}.

4.9. UV−Vis Light Absorption Spectroscopy. The UV−vis light spectra were measured using V-670 (JASCO) at room temperature. The sample used was a 5 wt % ionomer solution using DMAc as a solvent, which was spin-coated on a quartz substrate at 6000 rpm for 60 s.

4.10. DFT Calculation. DFT calculations were carried out with Materials Studio DMol^3 package (BIOVIA, version 2021). Further details can be found in the Supporting Information.

4.11. TEM. For TEM, the membranes were ion-exchanged by immersing in the $PtCl_4^{2-}$ aqueous solution. The membranes were rinsed with deionized water and dried in vacuum for 12 h. The stained membranes were embedded in epoxy resin and subsequently sectioned to 60 nm thickness with a microtome (Ultracut UCT, Leica). Each specimen was placed on copper grids. TEM images were taken with a transmission electron microscope (H-9500, Hitachi) with an accelerating voltage of 200 kV.

4.12. SAXS. The SAXS measurements of AEMs in Cl^- form were performed using a NANO-Viewer (Rigaku) with an environmental chamber.[47] As the X-ray source, Cu ($K\alpha$) was used. After the AEMs were treated in 1 M hydrochloric acid solution at room temperature for 48 h, they were subsequently immersed in deionized and degassed water for 24 h. The AEMs were then installed in the SAXS environmental chamber. Under a N_2 atmosphere, each specimen was equilibrated at least for 2 h at 40 °C and humidity between 30 and 90% before the SAXS measurements. The scattering patterns were obtained using a high-speed 2D detector (PILATUS 100 K/R, Rigaku).

4.13. CS-AFM. To avoid the absorption of CO_2, QPAF-(C4)-4 and QPAF(C6)-4 membranes were placed in 1 M KOH aqueous solution for 48 h and rinsed in deionized and degassed water for 24 h. The membranes, while still wet, were pressed at room temperature with gas diffusion electrodes (GDEs) prepared by spraying a catalyst ink containing Pt catalyst supported on carbon black (TEC10E50, 47.9 mass %-Pt, Tanaka Kikinzoku Kogyo), with ionomer (AS-5, Tokuyama Co.) as a binder on a GDL with a microporous layer (25 BC, SGL Carbon Group Co.) using a pulse−swirl−spray apparatus (Nordson).[32] The specimen was subsequently installed in an environmental chamber. Humidified air was continuously supplied to the chamber (dead volume = 500 mL) at 100 mL min^{-1} for 2 h before the measurements. During the AFM measurements, the flow rate was lowered to 10 mL min^{-1}.

CS-AFM measurements were carried out at 40 °C and 70% RH with a commercial AFM system (SPM-5500, Agilent) under ultrapure air (CO_2 less than 5 ppb).[48−53] OH^- ions formed at the cathode at a silicon AFM tip (Nanoworld) coated with Pt−Ir alloy were transferred to the anode through the AEM and oxidized to oxygen at the anode.[53] Topographic and current images were simultaneously obtained in the contact mode (contact force = 5 nN, tip voltage = −0.2 V). To ensure no tip damage, no membrane degradation, and no influence of carbonates, two identical images at the same position were obtained in the scanned range of 5 μm × 5 μm before the scanned area was decreased to 1 μm × 1 μm. The scanning rate was 0.6 line s^{-1}.

■ ASSOCIATED CONTENT

Supporting Information

The Supporting Information is available free of charge at https://pubs.acs.org/doi/10.1021/acsomega.1c06958.

Method of DFT calculations; MD geometries of two model molecules: correlations of energy; and wavelength and H−H distance (PDF)

■ AUTHOR INFORMATION

Corresponding Authors

Kenji Miyatake − *Fuel Cell Nanomaterials Center, University of Yamanashi, Kofu 400-0021, Japan; Clean Energy Research Center, University of Yamanashi, Kofu 400-8510, Japan; Department of Applied Chemistry, Waseda University, Tokyo 169-8555, Japan;* orcid.org/0000-0001-5713-2635; Email: miyatake@yamanashi.ac.jp

Junji Inukai − *Fuel Cell Nanomaterials Center, University of Yamanashi, Kofu 400-0021, Japan; Fuel Cell Institute, Universiti Kebangsaan Malaysia, Bangi, Selangor 43600, Malaysia; Clean Energy Research Center, University of Yamanashi, Kofu 400-8510, Japan;* orcid.org/0000-0002-7819-842X; Email: jinukai@yamanashi.ac.jp

Authors

Yuto Shirase − *Integrated Graduate School of Medicine, Engineering, and Agricultural Sciences, University of Yamanashi, Yamanashi 400-8510, Japan*

Akinobu Matsumoto − *Fuel Cell Nanomaterials Center, University of Yamanashi, Kofu 400-0021, Japan;* Present Address: INAMORI Frontier Research Center, Kyushu University, 744 Nishi-ku, Motooka, Fukuoka 819-0395, Japan

Kean Long Lim − *Fuel Cell Institute, Universiti Kebangsaan Malaysia, Bangi, Selangor 43600, Malaysia;* orcid.org/0000-0002-7227-5391

Donald A. Tryk − *Fuel Cell Nanomaterials Center, University of Yamanashi, Kofu 400-0021, Japan;* orcid.org/0000-0003-4660-9674

Complete contact information is available at: https://pubs.acs.org/10.1021/acsomega.1c06958

Notes

The authors declare no competing financial interest.

https://doi.org/10.1021/acsomega.1c06958
ACS Omega 2022, 7, 13577−13587

■ ACKNOWLEDGMENTS

This work was partly supported by the New Energy and Industrial Technology Development Organization (NEDO) of Japan through the fund for "Advanced Research Program for Energy and Environmental Technologies," Ministry of Education, Culture, Sports, Science and Technology (MEXT) through KAKENHI, Japan Science and Technology (JST) through SICORP and A-STEP, JKA foundation, Thermal and Electric Energy Technology Foundation, and Heiwa Nakajima Foundation.

■ REFERENCES

(1) Carrette, L.; Friedrich, K. A.; Stimming, U. Fuel Cells-Fundamentals and Applications. *Fuel Cells* **2001**, *1*, 5−39.
(2) Hickner, M. A.; Pivovar, B. S. The Chemical and Structural Nature of Proton Exchange Membrane Fuel Cell Properties. *Fuel Cells* **2005**, *5*, 213−229.
(3) Couture, G.; Alaaeddine, A.; Boschet, F.; Ameduri, B. Polymeric materials as anion-exchange membranes for alkaline fuel cells. *Prog. Polym. Sci.* **2011**, *36*, 1521−1557.
(4) Merle, G.; Wessling, M.; Nijmeijer, K. Anion exchange membranes for alkaline fuel cells: A review. *J. Membr. Sci.* **2011**, *377*, 1−35.
(5) Hickner, M. A.; Herring, A. M.; Coughlin, E. B. Anion exchange membranes: Current status and moving forward. *J. Polym. Sci., Part B: Polym. Phys.* **2013**, *51*, 1727−1735.
(6) Varcoe, J. R.; Atanassov, P.; Dekel, D. R.; Herring, A. M.; Hickner, M. A.; Kohl, P. A.; Kucernak, A. R.; Mustain, W. E.; Nijmeijer, K.; Scott, K.; Xu, T.; Zhuang, L. Anion-exchange membranes in electrochemical energy systems. *Energy Environ. Sci.* **2014**, *7*, 3135−3191.
(7) Gottesfeld, S.; Dekel, D. R.; Page, M.; Bae, C.; Yan, Y.; Zelenay, P.; Kim, Y. S. Anion exchange membrane fuel cells: Current status and remaining challenges. *J. Power Sources* **2018**, *375*, 170−184.
(8) Dekel, D. R. Review of cell performance in anion exchange membrane fuel cells. *J. Power Sources* **2018**, *375*, 158−169.
(9) Arges, C. G.; Zhang, L. Anion Exchange Membranes' Evolution toward High Hydroxide Ion Conductivity and Alkaline Resiliency. *ACS Appl. Energy Mater.* **2018**, *1*, 2991−3012.
(10) Park, E. J.; Kim, Y. S. Quaternized aryl ether-free polyaromatics for alkaline membrane fuel cells: synthesis, properties, and performance − a topical review. *J. Mater. Chem. A* **2018**, *6*, 15456−15477.
(11) Valade, D.; Boschet, F.; Ameduri, B. Random and Block Styrenic Copolymers Bearing Both Ammonium and Fluorinated Side-Groups. *J. Polym. Sci., Part A: Polym. Chem.* **2011**, *49*, 4668−4679.
(12) Cha, M.; Lee, J.; Kim, T.; Jeong, Y.; Shina, H.; Oh, S.; Hong, Y. Preparation and characterization of crosslinked anion exchange membrane (AEM) materials with poly(phenylene ether)-based short hydrophilic block for use in electrochemical applications. *J. Membr. Sci.* **2017**, *530*, 73−83.
(13) Luo, Y.; Guo, J.; Wang, C.; Chu, D. Quaternized poly(methyl methacrylate-co-butyl acrylate-co-vinylbenzyl chloride) membrane for alkaline fuel cells. *J. Power Sources* **2010**, *195*, 3765−3771.
(14) Gupta, G.; Scott, K.; Mamlouk, M. Soluble Polystyrene-b-poly (ethylene/butylene)-b-polystyrene Based Ionomer for Anion Exchange Membrane Fuel Cells Operating at 70 °C. *Fuel Cells* **2018**, *18*, 137−147.
(15) Tanaka, M.; Koike, M.; Miyatake, K.; Watanabe, M. Synthesis and properties of anion conductive ionomers containing fluorenyl groups for alkaline fuel cell applications. *Polym. Chem.* **2011**, *2*, 99−106.
(16) Zheng, J.; Zhang, Q.; Qian, H.; Xue, B.; Li, S.; Zhang, S. Self-assembly prepared anion exchange membranes with high alkaline stability and organic solvent resistance. *J. Membr. Sci.* **2017**, *522*, 159−167.
(17) Fan, J.; Cohen, S. W.; Schibli, E. M.; Paula, Z.; Li, W.; Skalski, T. J. G.; Sergeenko, A. T.; Hohenadel, A.; Frisken, B. J.; Magliocca, E.; Mustain, W. E.; Dekel, D. R.; Holdcroft, S. Poly(bis-arylimidazoliums) possessing high hydroxide ion exchange capacity and high alkaline stability. *Nat. Commun.* **2019**, *10*, 2306.
(18) Chen, W.; Mandel, M.; Huang, G.; Wu, X.; He, G.; Kohl, P. A. Highly Conducting Anion-Exchange Membranes Based on Cross-Linked Poly(norbornene): Ring Opening Metathesis Polymerization. *ACS Appl. Energy Mater.* **2019**, *2*, 2458−2468.
(19) Buggy, N. C.; Du, Y.; Kuo, M. C.; Ahrens, K. A.; Wilkinson, J. S.; Seifert, S.; Coughlin, E. B.; Herring, A. M. A Polyethylene-Based Triblock Copolymer Anion Exchange Membrane with High Conductivity and Practical Mechanical Properties. *ACS Appl. Polym. Mater.* **2020**, *2*, 1294−1303.
(20) Olsson, J. S.; Pham, T. H.; Jannasch, P. Poly(arylene piperidinium) Hydroxide Ion Exchange Membranes: Synthesis, Alkaline Stability, and Conductivity. *Adv. Funct. Mater.* **2018**, *28*, No. 1702758.
(21) Wang, L.; Brink, J. J.; Liu, Y.; Herring, A. M.; Ponce-Gonzalez, J.; Whelligan, D. K.; Varcoe, J. R. Non-fluorinated pre-irradiation-grafted (peroxidated) LDPE-based anion-exchange membranes with high performance and stability. *Energy Environ. Sci.* **2017**, *10*, 2154−2167.
(22) Pham, T. H.; Olsson, J. S.; Jannasch, P. Poly(arylene alkylene)s with pendant N-spirocyclic quaternary ammonium cations for anion exchange membranes. *J. Mater. Chem. A* **2018**, *6*, 16537−16547.
(23) Wang, J.; Li, S.; Zhang, S. Novel Hydroxide-Conducting Polyelectrolyte Composed of an Poly(arylene ether sulfone) Containing Pendant Quaternary Guanidinium Groups for Alkaline Fuel Cell Applications. *Macromolecules* **2010**, *43*, 3890−3896.
(24) Tanaka, M.; Koike, M.; Miyatake, K.; Watanabe, M. Anion Conductive Aromatic Ionomers Containing Fluorenyl Groups. *Macromolecules* **2010**, *43*, 2657−2659.
(25) Chen, N.; Long, C.; Li, Y.; Lu, C.; Zhu, H. Ultrastable and High Ion-Conducting Polyelectrolyte Based on Six-Membered N-Spirocyclic Ammonium for Hydroxide Exchange Membrane Fuel Cell Applications. *ACS Appl. Mater. Interfaces* **2018**, *10*, 15720−15732.
(26) Lai, A. N.; Guo, D.; Lin, C. X.; Zhang, Q. G.; Zhu, A. M.; Ye, M. L.; Liu, Q. L. Enhanced performance of anion exchange membranes via crosslinking of ion cluster regions for fuel cells. *J. Power Sources* **2016**, *327*, 56−66.
(27) Pan, J.; Han, J.; Zhu, L.; Hickner, M. A. Cationic Side-Chain Attachment to Poly(Phenylene Oxide) Backbones for Chemically Stable and Conductive Anion Exchange Membranes. *Chem. Mater.* **2017**, *29*, 5321−5330.
(28) Dang, H.; Jannasch, P. Exploring Different Cationic Alkyl Side Chain Designs for Enhanced Alkaline Stability and Hydroxide Ion Conductivity of Anion-Exchange Membranes. *Macromolecules* **2015**, *48*, 5742−5751.
(29) Zhu, L.; Pan, J.; Wang, Y.; Han, J.; Zhuang, L.; Hickner, M. Multication Side Chain Anion Exchange Membranes. *Macromolecules* **2016**, *49*, 815−824.
(30) Disabb-Miller, M. L.; Zha, Y.; DeCarlo, A. J.; Pawar, M.; Tew, G. N.; Hickner, M. A. Water Uptake and Ion Mobility in Cross-Linked Bis(terpyridine)ruthenium-Based Anion Exchange Membranes. *Macromolecules* **2013**, *46*, 9279−9287.
(31) Duan, Q.; Ge, S.; Wang, C.-Y. Water uptake, ionic conductivity and swelling properties of anion-exchange membrane. *J. Power Sources* **2013**, *243*, 773−778.
(32) Han, K. W.; Ko, K. H.; Abu-Hakmeh, K.; Bae, C.; Sohn, Y. J.; Jang, S. S. Molecular Dynamics Simulation Study of a Polysulfone-Based Anion Exchange Membrane in Comparison with the Proton Exchange Membrane. *J. Phys. Chem. C* **2014**, *118*, 12577−12587.
(33) Ponce-Gonzalez, J.; Ouachan, I.; Varcoe, J. R.; Whelligan, D. K. Radiation-induced grafting of a butyl-spacer styrenic monomer onto ETFE: the synthesis of the most alkali stable radiation-grafted anion exchange membrane to date. *J. Mater. Chem. A* **2018**, *6*, 823−827.
(34) Fan, J.; Wright, A. G.; Britton, B.; Weissbach, T.; Skalski, T. J. G.; Ward, J.; Peckham, T. J.; Holdcroft, S. Cationic Polyelectrolytes, Stable in 10 M KOH aq at 100 °C. *ACS Macro Lett.* **2017**, *6*, 1089−1093.

https://doi.org/10.1021/acsomega.1c06958
ACS Omega 2022, 7, 13577−13587

(35) Marino, M. G.; Kreuer, K. D. Alkaline stability of quaternary ammonium cations for alkaline fuel cell membranes and ionic liquids. *ChemSusChem* **2015**, *8*, 513−523.
(36) Hugar, K. M.; IV Kostalik, H. A.; Coates, G. W. Imidazolium Cations with Exceptional Alkaline Stability: A Systematic Study of Structure−Stability Relationships. *J. Am. Chem. Soc.* **2015**, *137*, 8730−8737.
(37) Ono, H.; Miyake, J.; Shimada, S.; Uchida, M.; Miyatake, K. Anion exchange membranes composed of perfluoroalkylene chains and ammonium-functionalized oligophenylenes. *J. Mater. Chem. A* **2015**, *3*, 21779−21788.
(38) Ozawa, M.; Kimura, T.; Akiyama, R.; Miyake, J.; Inukai, J.; Miyatake, K. Copolymers Composed of Perfluoroalkyl and Ammonium-Functionalized Fluorenyl Groups as Chemically Stable Anion Exchange Membranes. *Bull. Chem. Soc. Jpn.* **2017**, *90*, 1088−1094.
(39) Ozawa, M.; Kimura, T.; Otsuji, K.; Akiyama, R.; Miyake, J.; Uchida, M.; Inukai, J.; Miyatake, K. Structurally Well-Defined Anion Exchange Membranes Containing Perfluoroalkyl and Ammonium Functionalized Fluorenyl Groups. *ACS Omega* **2018**, *3*, 16143−16149.
(40) Ono, H.; Miyake, J.; Miyatake, K. Partially Fluorinated and Ammonium-Functionalized Terpolymers: Effect of Aliphatic Groups on the Properties of Anion Conductive Membranes. *J. Polym. Sci., Part A: Polym. Chem.* **2017**, *55*, 1442−1450.
(41) Mahmoud, A. M. A.; Elsaghier, A. M. M.; Otsuji, K.; Miyatake, K. High Hydroxide Ion Conductivity with Enhanced Alkaline Stability of Partially Fluorinated and Quaternized Aromatic Copolymers as Anion Exchange Membranes. *Macromolecules* **2017**, *50*, 4256−4266.
(42) Mahmoud, A. M. A.; Miyatake, K. Optimization of the pendant chain length in partially fluorinated aromatic anion exchange membranes for alkaline fuel cells. *J. Mater. Chem. A* **2018**, *6*, 14400−14409.
(43) Miyake, J.; Miyatake, K. Quaternized poly(arylene perfluoroalkylene)s (QPAFs) for alkaline fuel cells − a perspective. *Sustainable Energy Fuels* **2019**, *3*, 1916−1928.
(44) Ono, H.; Kimura, T.; Takano, A.; Asazawa, K.; Miyake, J.; Inukai, J.; Miyatake, K. Robust Anion Conductive Polymers Containing Perfluoroalkylene and Pendant Ammonium Groups for High Performance Fuel Cells. *J. Mater. Chem. A* **2017**, *5*, 24804−24812.
(45) Brydson, J. A. Relation of Structure to Thermal and Mechanical Properties. In *Brydson's Plastics Materials*, 8th ed.; View A; Butterworth-Heinemann: United Kingdom, 2017; pp 59−73.
(46) Peterlin, A. Molecular model of drawing polyethylene and polypropylene. *J. Mater. Sci.* **1971**, *6*, 490−508.
(47) Mochizuki, T.; Kakinuma, K.; Uchida, M.; Deki, S.; Watanabe, M.; Miyatake, K. Temperature- and humidity-controlled SAXS analysis of proton-conductive ionomer membranes for fuel cells. *ChemSusChem* **2014**, *7*, 729−733.
(48) Hara, M.; Kimura, T.; Nakamura, T.; Shimada, M.; Ono, H.; Shimada, S.; Miyatake, K.; Uchida, M.; Inukai, J.; Watanabe, M. Effect of surface ion conductivity of anion exchange membranes on fuel cell performance. *Langmuir* **2016**, *32*, 9557−9565.
(49) Hara, M.; Hattori, D.; Inukai, J.; Bae, B.; Hoshi, T.; Hara, M.; Miyatake, K.; Watanabe, M. Imaging individual proton-conducting spots on sulfonated multiblock-copolymer membrane under controlled hydrogen atmosphere by current-sensing atomic force microscopy. *J. Phys. Chem. B* **2013**, *117*, 3892−3899.
(50) Hara, M.; Daiki, H.; Inukai, J.; Hara, M.; Miyatake, K.; Watanabe, M. Reversible/irreversible increase in proton-conductive areas on proton-exchange-membrane surface by applying voltage using current-sensing atomic force microscope. *J. Electroanal. Chem.* **2014**, *716*, 158−163.
(51) Hara, M.; Hara, M.; Miyatake, K.; Inukai, J.; Watanabe, M. Effects of hot liquid-water treatment on local proton conductivity at surfaces of sulfonated poly(arylene ketone) block copolymer membrane for fuel cells studied by current-sensing atomic force microscopy. *Electrochim. Acta* **2014**, *143*, 383−389.
(52) Hara, M.; Miyahara, T.; Hoshi, T.; Ma, J.; Hara, M.; Miyatake, K.; Inukai, J.; Alonso Vante, N.; Watanabe, M. Proton conductive areas on sulfonated poly(aryleneketone) multiblock copolymer electrolyte membrane studied by current-sensing atomic force microscopy. *Electrochemistry* **2014**, *82*, 369−375.
(53) Kimura, T.; Akiyama, R.; Miyatake, K.; Inukai, J. Phase separation and ion conductivity in the bulk and at the surface of anion exchange membranes with different ion exchange capacities at different humidities. *J. Power Sources* **2018**, *375*, 397−403.
(54) Sheen, H. T.; Kahler, H. L. Effect of ions on Mohr method for chloride determination. *Ind. Eng. Chem. Anal. Ed.* **1938**, *10*, 628.

https://doi.org/10.1021/acsomega.1c06958
ACS Omega 2022, 7, 13577−13587